algorithms

MDPI

Article

Optimal Design Parameters for Hybrid DC Circuit Breakers Using a Multi-Objective Genetic Algorithm

Van-Vinh Nguyen [1], Nhat-Tung Nguyen [1], Quang-Thuan Nguyen [1], Van-Hai Bui [2,*] and Wencong Su [3,*]

[1] Department of Electrical and Electronic Engineering, Thuyloi University, 175 Tay Son, Hanoi 100000, Vietnam
[2] Department of Electrical Engineering, (SUNY) Maritime College, State University of New York, Bronx, NY 10465, USA
[3] Department of Electrical and Computer Engineering, University of Michigan-Dearborn, Dearborn, MI 48128, USA
* Correspondence: vhbui@sunymaritime.edu or vhbui@umich.edu (V.-H.B.); wencong@umich.edu (W.S.); Tel.: +1-734-686-1940 (V.-H.B.); +1-313-593-5314 (W.S.)

Abstract: The primary function of hybrid direct current circuit breakers (HCBs) is to quickly interrupt fault currents to protect high-voltage direct current (HVDC) systems. To enhance the reliability and stability of HVDC systems, optimal design of HCBs is required to minimize the peak fault current, interruption time, and recovery time. Therefore, this study develops a multi-objective genetic algorithm (MOGA)-based optimization model to identify the optimal parameters for HCBs. The MOGA model consists of three objective functions that provide trade-offs among reductions in the peak fault current, the interruption time, and the recovery time. The proposed algorithm is verified with a novel HCB topology using inverse current injection techniques. The performance of the HCB topology with the optimal parameters is validated in the MATLAB/Simulink environment. In addition, a comparison study between the optimal design of an HCB using the proposed algorithm and a typical HCB model is presented in this study to show the effectiveness of the proposed optimization method. Our simulation results show that the optimal parameter design of HCBs significantly reduces the magnitude of the peak fault current and operating time, thus maintaining the safe and stable operation of the entire system.

Keywords: high-voltage direct current (HVDC) grid; hybrid circuit breaker (HCB); multi-objective genetic algorithm (MOGA)

Citation: Nguyen, V.-V.; Nguyen, N.-T.; Nguyen, Q.-T.; Bui, V.-H.; Su, W. Optimal Design Parameters for Hybrid DC Circuit Breakers Using a Multi-Objective Genetic Algorithm. *Algorithms* **2022**, *15*, 298. https://doi.org/10.3390/a15090298

Academic Editor: Abdulsalam Yassine

Received: 22 July 2022
Accepted: 14 August 2022
Published: 25 August 2022

1. Introduction

High-voltage direct current (HVDC) systems have been widely used in power systems due to their outstanding advantages, such as high efficiency and low electrical losses [1–3]. However, the major challenge with HVDC systems is the isolation of DC faults, because there are no natural zero-crossing points in the currents. When faults occur in HVDC systems, the components of the HVDC systems can become damaged due to the significant increase in fault currents within a short time [4,5]. To minimize the damage and ensure stable system operation, DC faults should be quickly isolated from HVDC systems. DC circuit breakers (DCCBs) have been widely applied to isolate fault currents in these systems [6].

DCCB technologies can be classified into three types: mechanical DCCBs (MCBs) [7–9], semiconductor-based DCCBs (SCBs) [10–13], and hybrid DCCBs (HCBs) [14–21]. Out of these three types of DCCBs, HCBs have attracted the most attention for applications in HVDC systems because they offer the advantages of both MCBs and SCBs, especially the HCBs that were proposed by ABB and Alstom. However, these topologies have high capital costs, especially in meshed HVDC grids. Therefore, another type of HCB that is

based on the inverse current injection method with the use of thyristors has been considered as an attractive alternative. Nevertheless, such HCBs use passive elements, such as resistors, inductors, and capacitors. Since they can increase peak fault currents, the interruption time, and the recovery time, these elements should be optimized to enhance the overall performance of the HCBs.

Several ways of optimizing the parameters of DCCB topologies have been investigated [22–25]. An optimization algorithm was proposed in [22] that ensured that fault currents could be interrupted when the derivatives of injected currents were lower than a critical value. However, the proposed algorithm in [22] was limited to mechanical DCCBs and was not able to be applied in HCBs. This is because HCBs include switching components, such as semiconductors and thyristors, so it is difficult to obtain exact models of HCBs to identify their optimal design. To overcome this problem, genetic algorithms (GAs) employing the heuristic search and optimization technique have been used for the design of HCBs. In [23], a GA was used to find the breaking time and the commutation capacitor voltage. The optimal design of DCCBs can ensure that commutation branches can successfully transfer main currents to the commutation branches. A multi-objective optimization model was proposed in [24] that used a GA to minimize the commutation circuit parameters and reduce the development time. Another GA-based algorithm was proposed in [25] for the optimal design of HCBs. This algorithm aimed to minimize the energy capacity of the commutation capacitor and the parameters of the thyristors, such as voltage and current.

Most previous studies on the optimal design of HCBs have focused on minimizing the commutation branches, such as the energy capacity of capacitors, the capacitor voltage, and the thyristor current or voltage. However, many other parameters that are also important, including peak fault current, interruption time, and recovery time, have not received enough attention. Reducing the magnitude of peak fault currents can avoid the damage that is caused by extremely high fault currents in systems, while reducing the interruption time significantly improves system stability and quickly isolates fault areas. In addition, the recovery time, which is the time that is required for the HCB to become ready for the next interruption, should also be considered to avoid the long-term interruption of power to connected AC grids. To achieve these goals, this study developed a multi-objective optimization model that uses a GA to minimize the peak fault current, interruption time, and recovery time. The GA can handle both discrete and continuous variables and can also solve complex optimization problems [26]. Therefore, the proposed multi-objective GA is very efficient at identifying the optimal design parameters of HCB topologies [27]. The proposed optimization model mimics the process of natural evolution, and the weighted sum method is used to analyze the impact of each objective function. The HCB that was proposed in [21] is used in this study to show the effectiveness of our proposed optimization model. The HCB model is simulated in the Simulink environment, while the MOGA is implemented as a MATLAB function. Finally, a comparison study between the optimal and initial parameters of the HCBs is also presented in detail. The major contributions of this study are as follows:

- A MOGA-based optimization model that can optimally design the parameters of HCB topologies, which aims to achieve a trade-off between reducing the peak fault current, interruption time, and recovery time.
- A MOGA that allows the proposed model to handle both discrete and continuous variables, and therefore solve complex optimal design problems.
- An in-depth comparison study between the initial and optimal parameters of HCB topologies, the results of which showed that the proposed method provided the optimal parameters for the HCB topologies, and therefore significantly reduced the peak value of the fault current, the interruption time, and the recovery time.

This paper is organized as follows. Section 2 summarizes the configuration, working principles, and problem statement of our HCB topology. Section 3 discusses the proposed

MOGA, which is based on the weighted sum method. Section 4 presents the simulation results and the comparison. Finally, the main conclusions are presented in Section 5.

2. HCB Topology and Problem Statement

2.1. HCB Topology

2.1.1. Configuration of the HCB

The configuration of an HCB, which consists of five main branches in series with a residual switch S_1 and DC inductor L_{dc}, is shown in Figure 1. The nominal current branch (1) uses a fast mechanical switch S_1, which conducts the current under normal conditions. When a fault occurs on the load side, the switch S_1 is opened, which leads to the establishment of an arc between two contacts. To extinguish the arc in switch S_1, the commutation current branch (2), including an inductor L_p and a precharged capacitor C_p, injects an inverse current by turning on the pair of thyristors T_{1a-1b} or T_{2a-2b}. When the arc is extinguished, the fault current is commutated into the commutation current branch. Simultaneously, the transient interruption voltage (TIV), which is across the HCB terminals, increases rapidly along with the capacitor voltage. If the TIV is higher than the action level of the energy absorption branch (3), the metal oxide varistor (MOV) conducts the fault current and dissipates energy until the fault current reduces to zero. The residual switch S_1 is opened and the fault is cleared. Since the capacitor voltage is higher than the system voltage after clearing the fault, the discharging branch (4) consisting of a resistor R and a high-speed switch S_3 is used to reduce the capacitor voltage to the system voltage. Finally, the reversing branch (5) changes the polarity of the capacitor voltage with an inductor L and a thyristor T_3 to get the HCB ready for the next interruption.

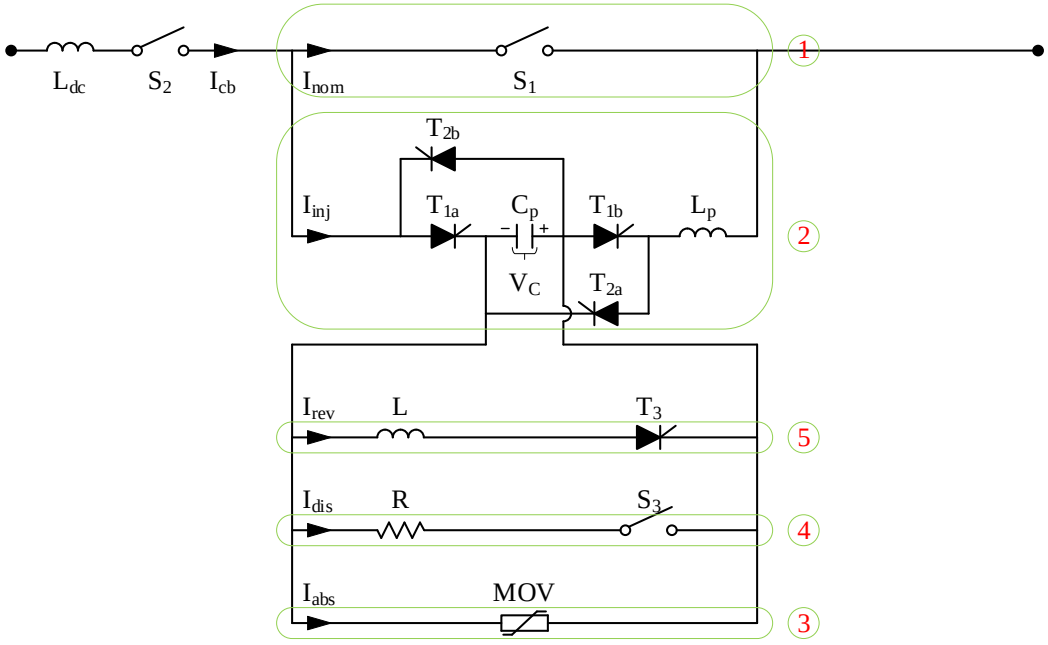

Figure 1. Configuration of the HCB

2.1.2. Working Principle of the HCB

The working principle of the HCB is shown in Figure 2. Under normal operation (before t_0), the switches S_1 and S_2 and thyristors T_1 and T_2 are closed, switch S_3 and thyristor T_3 are opened, and the capacitor C is precharged to the DC system voltage by an external circuit. The polarity of the capacitor voltage is opposite to the DC system voltage. The DC system current I_{dc} flows only through the nominal current branch (branch 1) and brings a nominal current I_{nom} = 1kA.

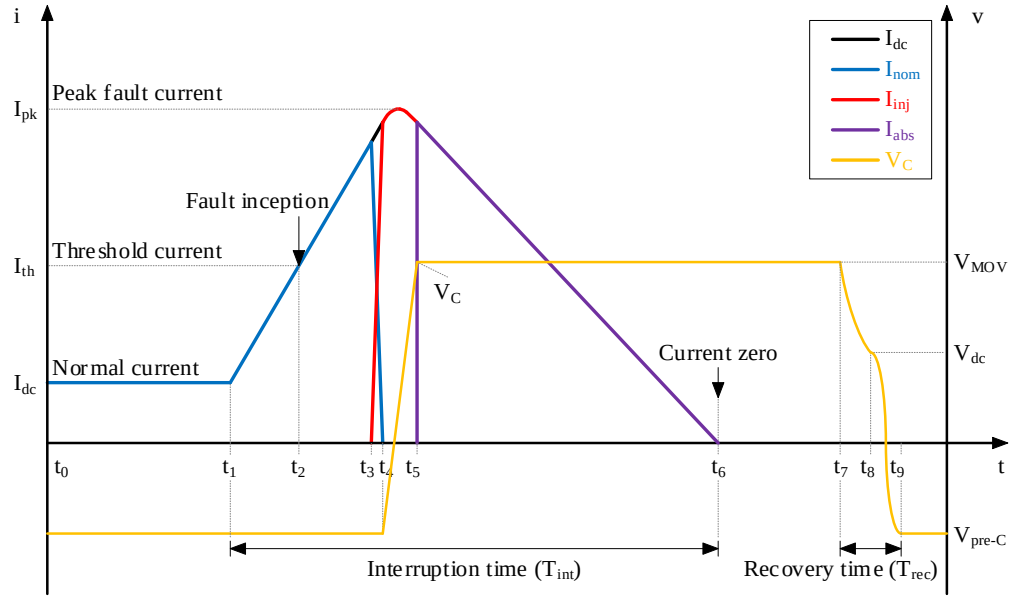

Figure 2. Waveform of current and voltage in the branches of the HCB

It is assumed that a fault occurs at t_1, and the system current starts to increase rapidly. When the magnitude of the fault current is larger than a predefined threshold I_{th} at t_2, the fault is detected. A trip signal is sent to the HCB, and the mechanical switch S_1 begins to open at t_2, resulting in an arc current between its contacts. After a delay time of the mechanical switch S_1 at t_3, the L_pC_p-resonant circuit in the commutation current branch (branch 2) injects an inverse current by turning on the thyristors T_{1a-1b} or T_{2a-2b} (depending on the current direction). Consequently, the increase in the current through branch 2 equals the decrease in the current through the mechanical switch S_1 $(t_3 - t_4)$. After the current through the mechanical switch S_1 reaches the current zero at t_4, the arc is extinguished. The fault current immediately commutates into branch 2 and re-charges the capacitor from $t_4 - t_5$. Thus, when the voltage across the breaker appears, the transient interruption voltage (TIV) between the terminals of the HCB starts to build up (from $t_4 - t_5$) to a protection voltage of the MOV at t_5. This makes the fault current commutate to the energy absorption branch (branch 3). During the period $t_5 - t_6$, the MOV absorbs the energy stored in the system. When the current flow of the circuit breaker I_{cb} passes through zero at t_6, the residual switch S_2 becomes an open circuit to clear the residual current and isolation of the HCB from the rest of the system. The fault current interruption is finished.

To enable multiple reclosing operations in rapid succession, a secondary inverse current injection circuit should be implemented. Therefore, the capacitor voltage needs to return to the nominal condition. This results in a discharging capacitor circuit to reduce the overvoltage down to the DC voltage. This mode is carried out at t_7. Then, a circuit of reversing capacitor voltage is applied to change the polarity of the capacitor voltage at t_8. This mode is completed at t_9, and the HCB is ready for the next operation. Table 1 summarizes the sequence of operation of the HCB.

Table 1. Summarizing sequence of operation of the HCB

States	Definition and Operation	Time
Normal operation	Breaker operates in normal conduction condition: • S_1 and S_2 have closed. • System current flows through S_1 and brings a nominal current.	$t_0 \leq t < t_1$

Fault inception	Fault current arrives at the circuit breaker location: • Current increases. • DC side voltage starts to drop.	$t = t_1$
Relay time	Time for fault detection: • Breaker receives trip signal sent from system. • Switch S_1 begins to open first.	$t_1 \leq t < t_2$
Fault interruption	After a delay time of switch S_1: • Switch S_1 has opened. • Thyristors T_{1a-1b} or T_{2a-2b} have closed. • A current zero is generated in S_1 from the L_pC_p resonant circuit. • The capacitor is charged until it reaches the MOV clamping voltage. • Current is then commutated into the MOV. • MOV absorbs the energy stored in the system.	$t_2 \leq t \leq t_6$
Residual switch open	Residual current circuit breaker (S_2) opens: • Current has reached leakage level (several mA). • Residual current is removed by S_2.	$t_6 \leq t \leq t_7$
Discharging operation	Capacitor is discharged to the system voltage.	$t_7 \leq t \leq t_8$
Reversing operation	Polarity of the capacitor is changed and opposite to the system voltage.	$t_8 \leq t \leq t_9$

2.2. Problem Statement

Based on the explanation of the configuration and working principles of the HCB, it is obvious that the performance of the HCB depends directly on the parameters design of the commutation branch with the L_p and C_p elements, the discharging branch with the R element, and the reversing branch with the L element. These elements should be optimal parameters to satisfy the operation requirements of the HCB for HVDC grid application. Consequently, the HCB should have a low amplitude of fault current as well as the operation speed of fault current interruption and recovery time. Hence, in order to optimize parameters of the HCB, the operation of the HCB needs to minimize the peak fault current, interruption time, and recovery time. Each of the above characteristics is considered an objective function to determine the optimal values of HCB parameters (i.e., R, L, L_p, C_p) [21,28], and can be calculated as.

- Peak fault current (I_{pk}) is the maximum value of the fault current flowing through the HCB during fault current interruption. The fault current is computed by tracking the fault current, as given in (1).

$$f_1 = I_{pk} = \text{Peak}\{i_{dc}(t)\} \quad (1)$$

- Interruption time (T_{int}) is the total time to clear the short-circuit fault from the grid. This time period is determined from fault inception ($t = t_1$) until fault clearing ($t = t_6$) and can be given as (2).

$$f_2 = T_{int} = t_6 - t_1 \quad (2)$$

- Recovery time (T_{rec}) is the total time to recover the capacitor voltage to normal condition. This period starts from the discharge mode ($t = t_7$) until the reverse mode ends ($t = t_9$) and can be computed by (3).

$$f_3 = T_{rec} = t_9 - t_7 \quad (3)$$

In this study, a multi-objective function model is developed using the three objective functions (1) to (3) to optimize the parameter design of the HCB. The detailed procedure for implementation of the proposed MOGA is described in the following section.

3. Parameters Optimization Using Multi-Objective Genetic Algorithm

3.1. Multi-Objective Formulation

The optimal values of the HCB parameters are found using a multi-objective formulation that includes the objective functions (1) to (3). Weighting factors are used to combine the objective functions into a single objective function [29]. Furthermore, normalization is required in order to consistently combine objective functions (1) to (3). The objective function is formulated in (4).

Minimize

$$f'(x) = \sum_{i=1}^{3} w_i f_i'(x) = w_1 f_1'(x) + w_2 f_2'(x) + w_3 f_3'(x) \quad (4)$$

$$f_i'(x) = \frac{f_i(x) - f_{i,min}}{f_{i,max} - f_{i,min}} \text{ and } 0 \le f_i'(x) \le 1$$

Subject to

$$x = (x_1, x_2, \ldots, x_n) \in \Omega$$

$$\sum_{i=1}^{3} w_i = 1 \text{ and } 0 \le w_i \le 1$$

where $f_i'(x)$ is the normalized objective function $f_i(x)$, $f_{i,min}$ and $f_{i,max}$ are the minimum and maximum values for the i^{th} objective function $f_i(x)$, and x is a sample of individuals containing n design parameters of the HCB. The Ω represents the constraint sets for x. The weight coefficient w_i is a non-negative value corresponding to the i^{th} objective function, and it determines the contribution of each objective function to the global objective. Accordingly, in order to prevent damages to the system, the operation of the HCB should minimize the magnitude of the fault current and the interruption time. In contrast, up to 50 ms is allowed for the recovery time of the HCB after the fault clearance [30]. Therefore, the weight coefficients of I_{pk} and T_{int} should be larger than that of T_{rec}, and the weight coefficients are selected as follows $(w_1, w_2, w_3 = 0.45; 0.45; 0.1)$.

3.2. Operation Constraints

In order to interrupt a fault current, the inverse current of the resonant circuit in the commutation branch is defined by [31].

$$i_{inj}(t) = V_{pre-c}\sqrt{\frac{C_p}{L_p}}\sin\frac{1}{\sqrt{L_p C_p}}t \quad (5)$$

where $i_{inj}(t)$ is a function of current in the time domain, V_{pre-c} is the voltage value of the precharged capacitor. L_p and C_p are the inductor and capacitor elements of the commutation branch, respectively.

From Equation (5), the maximum slope and maximum amplitude of the resonant circuit current in the commutation branch are computed by (6) and (7), respectively.

$$\frac{di_2}{dt} = \frac{V_{pre-c}}{L_p} \quad (6)$$

$$I_{inj,max} = V_{pre-c}\sqrt{\frac{C_p}{L_p}} \quad (7)$$

In addition, in order to generate an artificial current zero, the magnitude of the inverse current of the L_pC_p resonant circuit in the commutation current branch should be greater than $K.I_{th}$. Hence, the maximum amplitude of the inverse current in the commutation branch is computed by (8).

$$I_{inj,max} = K.I_{th} \quad (8)$$

where K denotes the safety margin required to ensure successful interruption and HCB reliability.

Substituting Equation (8) into Equation (7) by replacing the $I_{inj,max}$ in (7) with $K.I_{th}$ from (8), Equation (8) is rearranged as

$$K.I_{th} = V_{pre-c}\sqrt{\frac{C_p}{L_p}} \quad (9)$$

Combining Equations (6) and (9), inductor L_p and capacitor C_p for the injected current can be determined as

$$L_p = \frac{V_{pre-c}}{di_{inj}/dt} \quad (10)$$

$$C_p = \frac{1}{di_{inj}/dt}\frac{(K.I_{th})^2}{V_{pre-c}} \quad (11)$$

where the threshold current I_{th} is set to 3 kA, the coefficient K is set to two for a 100% margin [32], and the boundary of the injected current slope di/dt is required for a successful arc extinction between $15\ A/\mu s$ and $200\ A/\mu s$ [33].

The resistor R and inductor L are calculated using (12) and (13), respectively.

$$R = \frac{T_d}{C_p} \quad (12)$$

$$L = \frac{T_r^2}{C_p} \quad (13)$$

where T_d is time to reduce the capacitor voltage to the DC system voltage (discharging capacitor voltage) and T_r is the time needed to change the polarity of the capacitor voltage (reversing capacitor voltage).

From Equation (10) to Equation (13), the ranges of the design parameters for the HCB model are tabulated in Table 2.

Table 2. Ranges of values for the HCB parameters

Parameter (Unit)	Range of Values
R (Ω)	40–80
L (mH)	2–40
L_p (mH)	0.3–6.67
C_p (uF)	1.8–24

3.3. Process of the Proposed MOGA

The MOGA mimics the process of natural selection to find the optimal solutions of optimal parameter design problems. Figure 3 shows the flowchart of the proposed MOGA for optimizing the parameters of the HCB. First, a set of input data (i.e., maximum generation; population size; constraint conditions; weight coefficients; and three operation probabilities of selection, crossover, and mutation) is initialized. Then, a population of individuals is normalized, where each individual consists of the values of parameters in the HCB topology (i.e., R, L, L_p, C_p). These values are randomly generated using a uniform distribution with a lower and upper bound. For instance, the individual i is shown by the vector $X_i = [R_i, L_i, L_{p,i}, C_{p,i}]$. The value of parameter $X_i[k]$ is determined by Equation (14), where k is the index of the vector X_i, α is generated randomly between [0, 1], and $X_{i,min}[k]$ and $X_{i,max}[k]$ are the lower and upper bounds of parameter k^{th} of individual X_i.

$$X_i = X_{i,min}[k] + \alpha\left(X_{i,max}[k] - X_{i,min}[k]\right) \quad (14)$$

To evaluate an individual, the values of design parameters are implemented in the dynamic model of the HCB in the MATLAB/Simulink environment, and then the output signals for HCB operation, including the interruption time, recovery time, and peak fault current, are measured. These results are used to calculate the fitness function, as given in Equation (15). The value of the fitness function determines the chance of selecting an individual for the next generation (i.e., selection and crossover).

$$F(x) = \frac{1}{f'(x)} \quad (15)$$

The individuals with higher fitness value have a higher probability of remaining in the next generation. This can be achieved via a selection operation with the roulette wheel approach, as expressed by Equation (16), in which the area of each segment is proportional to the fitness value of the individual. Then, the roulette wheel is spun a number of times that is equal to the population size to select the individuals with the highest fitness value. The selected individuals (parents) will go through crossover and mutation operations to produce new individuals (children).

$$p_s = \frac{F(x)}{\sum_{i=1}^{n} F(x)} \quad (16)$$

Crossover operation combines two parents (p_1 and p_2) and produces children (c_1 and c_2) for the next generation. This process is carried out by using a single-point crossover, and the crossover probability is the set of $p_c = 0.8$. We often choose a random value (p_r) between [0, 1] and compare it with the crossover probability. If $p_r \leq p_c$, the crossover is performed. The crossover point on both parents is randomly generated between [1, 4]. It determines the number of parameters that are taken from each parent. The parameters preceding the crossover point are copied from p_1 to c_1 and from p_2 to c_2. The parameters of p_1 following the crossover point are placed in the corresponding positions in c_2 and vice versa for the remaining parameters of p_2. Otherwise, if $p_r > p_c$, the parameters of p_1 and p_2 are directly copied into c_1 and c_2, respectively.

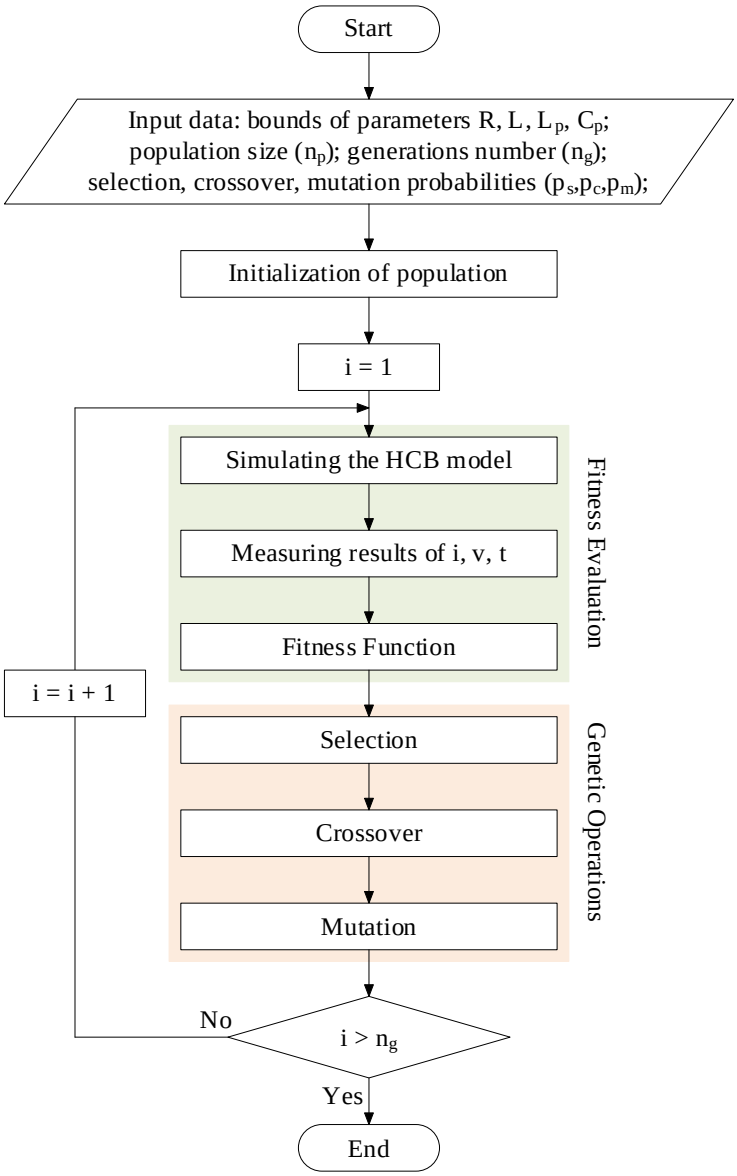

Figure 3. Flowchart of the proposed MOGA for optimizing parameters in the HCB

In order to avoid local optimal solutions and to explore new search areas, a mutation operation is randomly applied to a group of parents to generate children. In this process, we generate a random number in the range of [0, 1], and the mutation probability is the set of $p_m = 0.2$ to mutate the selected individual. If $p_r \leq p_c$, mutation is performed by random parameters according to the uniform distribution.

The algorithm iterates until the value of the multi-objective function $f'(x)$ converges or the number of iterations reaches a predefined value. Finally, the best individual is found as the optimal solution of the design problem.

4. Simulation Results

4.1. Test System

To optimize the parameters of the HCB topology in [21] using the proposed MOGA, the configuration and system implementation of the HCB are shown in Figure 4. The proposed model has been implemented in MATLAB/Simulink on a computer with an Intel (R) Core (TM) i5-7200U CPU @ 2.50 GHz and 32 GB of RAM memory. The simulation model parameters are provided in Table 3 for the HCB model and Table 4 for the MOGA model.

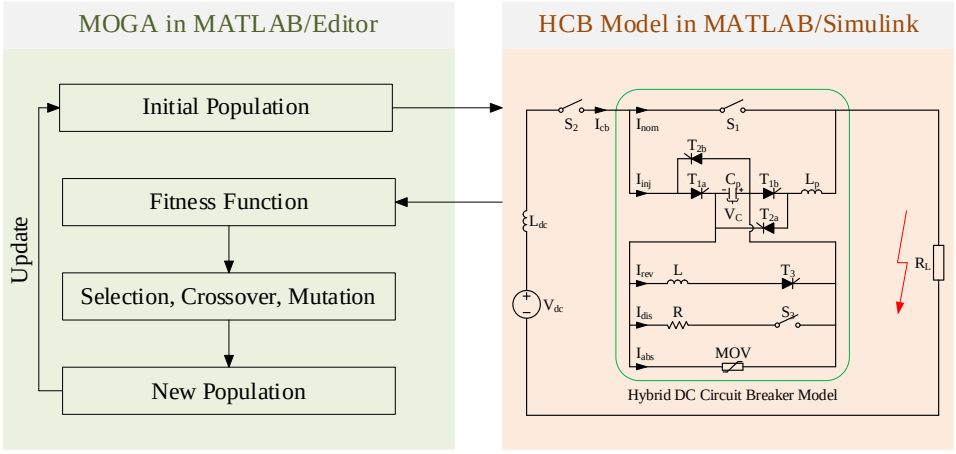

Figure 4. Configuration of the test system for optimizing parameters in the HCB

Table 3. Parameters of the HCB

Component	Symbol	Value
Rated DC voltage	V_{dc}	100 kV
Rated DC current	I_{dc}	1 kA
System inductance	L_{dc}	50 mH
Capacitor precharge voltage	V_{pre-c}	−100 kV
Load resistance	R_L	100 Ω
Threshold current	I_{th}	3 kA
Protection voltage level	V_{MOV}	200 kV

Table 4. Parameters of the MOGA

Parameters	Type	Value
Population size (n_p)	Randomly normalized	30
Selection probability (p_s)	Roulette wheel	2/30
Crossover probability (p_c)	Single point	0.8
Mutation probability (p_m)	Uniform random	0.2
Stopping criteria (n_g)	Number of generations	500

4.2. Results and Analysis

4.2.1. Results of optimizing parameters for the HCB by using the MOGA

The convergence process of the objective functions is shown in Figure 5, and the total computation time for the whole training process is about 2 h. The multi-objective value with the sum of three values of objective functions is shown in Figure 5a. The single-objective values are represented in Figure 5b–d. The value of objective function 1 represents the peak fault current, objective function 2 represents the interruption time, and objective function 3 represents the recovery time. It is obvious that the convergence curve of the objective functions decreases with an increasing number of generations. Initially, the multi-objective value is evaluated based on the initial population, and therefore the multi-objective value is high at 0.38, but as the number of generations increases, the multi-objective value improves due to the application of the three operations of selection, crossover, and mutation in the MOGA procedure. This continues until, at 200 generations, the optimal solution is found. With the optimal solution, the model has a multi-objective value equal to 0.016. As a result, the optimal values of the HCB parameters are [R, L, L_p, C_p] = [54 (Ω), 3.74 (mH), 0.32 (mH), 2.63 (uF)].

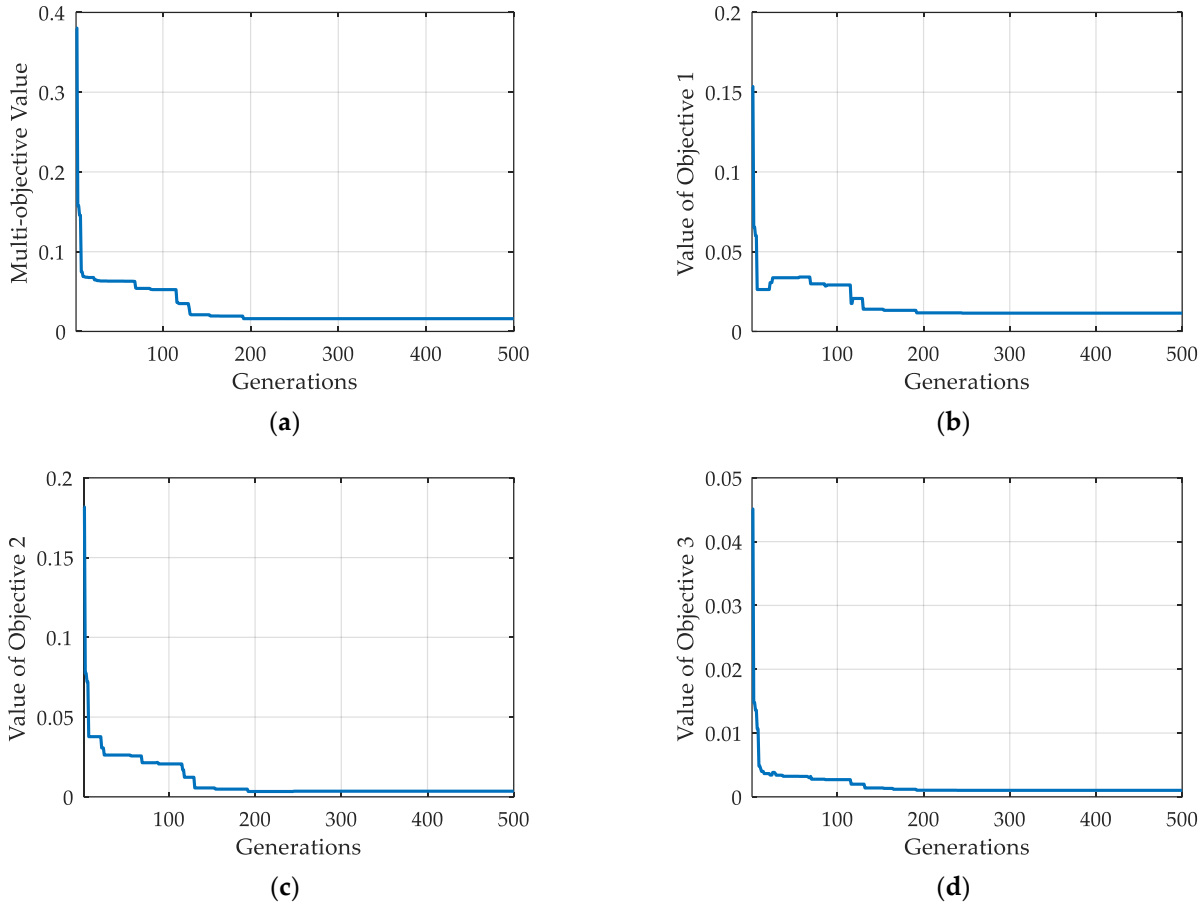

Figure 5. Convergence curve of: (**a**) multi-objective value, (**b**) value of objective 1, (**c**) value of objective 2, (**d**) value of objective 3

4.2.2. Comparison of using the initial and optimized parameters of the HCB

The performance of the HCB using the optimized parameters and the initial parameters is compared. Figures 6–10 show the simulation results of the current and voltage waveforms of the branches in the HCB. Figure 6 depicts the total current I_{cb} of the component currents in the HCB branches.

Under normal operation (before 0.04 s), the capacitor C is precharged to −100 kV, and the system current flows through switch S_1 in branch 1 with a nominal current of 1 kA, as shown in Figures 6 and 7.

When a fault occurs on the load side at 0.04 s, the system current increases rapidly. When the system current reaches the 3 kA threshold, an open signal is sent to switch S_1, and its contacts generate an arc. After a 2 ms delay, thyristors T_{1a} and T_{1b} are turned on, and the inverse current I_{inj} generated by the L_pC_p resonant circuit in branch 2 is injected to oppose the arc current. As a result, the current I_{nom} in branch 1 decreases to zero and the arc extinguishes at 0.04315 s for both cases, using the optimized and initial parameters, as shown in Figure 7. The fault current is commutated into branch 2. The voltages across the MS V_{ms} and the capacitor V_C increase rapidly at the same time, as shown in Figures 9 and 10. When the increasing V_{ms} equals the system voltage, the peak fault current is 7.56 kA for the initial parameters and 6.75 kA for the optimized parameters. Continuously, the increasing V_{ms} exceeds the turn-on voltage of the MOV at 0.044 s for the initial parameters and at 0.04323 s for the optimized parameters, and the fault current is commutated to the MOV in branch 3. The MOV absorbs the remaining fault energy in the system until the fault current is reduced to zero at 0.04743 s for the initial parameters and at 0.04645 s for the optimized parameters, as shown in Figure 8. It is obvious that the total

time of fault current interruption from fault inception to fault clearing is 7.43 ms (from 0.04 ms to 0.04743 ms) for the initial parameters and 6.45 ms (from 0.04 ms to 0.04645 ms) for the optimized parameters.

After the fault current interruption is completed, switch S_2 is fully opened after 20 ms at 0.06743 s for the initial parameters and at 0.06645 s for the optimized parameters, as shown in Figure 10. The HCB is isolated from the rest of the system. To resume operation, the HCB must recover from the overvoltage on the capacitor element. This process begins with the discharge of the capacitor overvoltage to the system voltage. This process takes 0.54 ms with initial parameters and 0.056 ms with optimized parameters, as shown in Figure 10. Furthermore, the polarity of the capacitor is reversed in comparison to the normal condition, so the capacitor polarity is changed. In this study, the process takes 1.984 ms with the initial parameters and 0.275 ms with the optimized parameters. The recovery time to the normal condition of the capacitor after the discharging and reversing operations is 2.52 ms for the initial parameters and 0.37 ms for the optimized parameters.

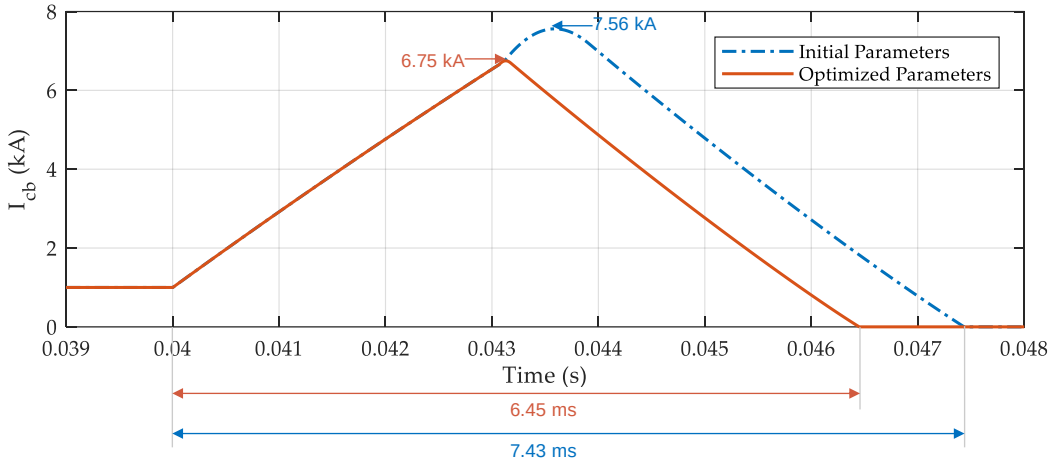

Figure 6. Current waveform of I_{cb} of the HCB

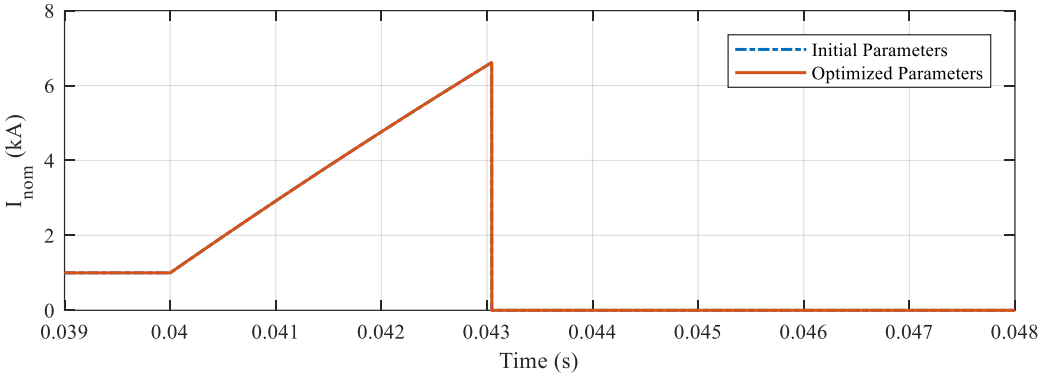

Figure 7. Current waveform of I_{nom} in branch 1 of the HCB

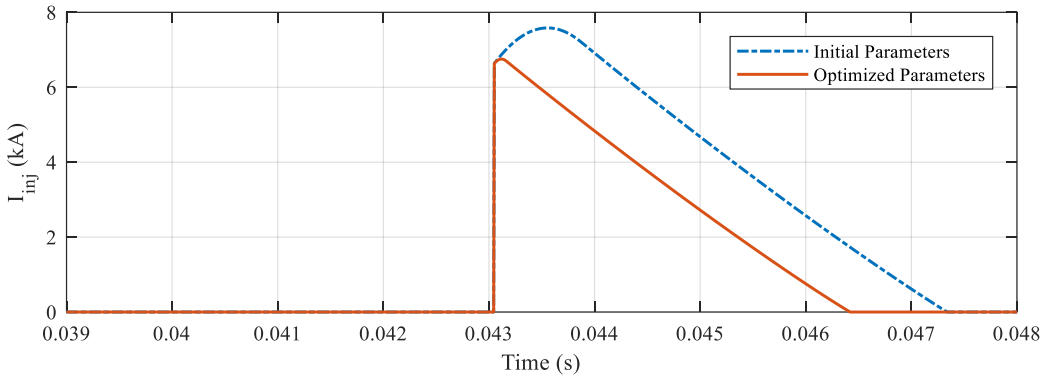

Figure 8. Current waveform of I_{inj} in branch 2 of the HCB

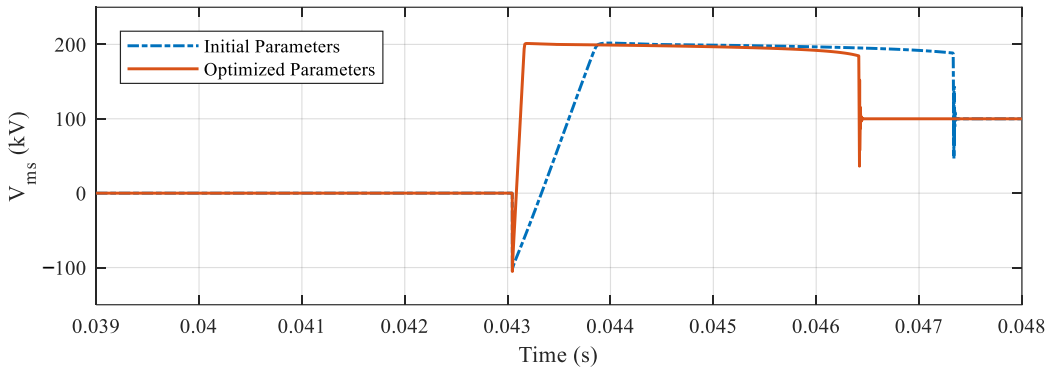

Figure 9. Voltage waveform of MS in branch 1 of the HCB

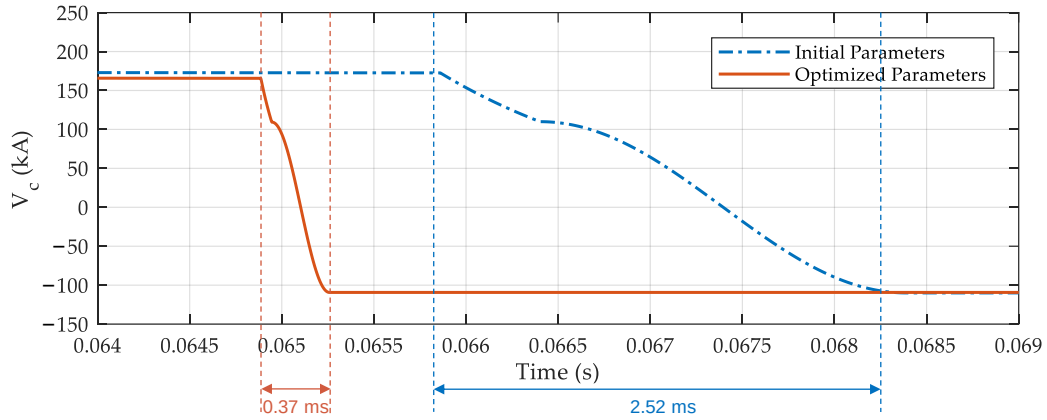

Figure 10. Voltage waveform of C in branch 2 of the HCB

Clearly, the performance of the HCB with optimal parameters exceeds that of the HCB model in [21], as shown in Table 5. Using the optimal parameters, the peak value of the fault current is reduced by 5.66% (from 7.56 kA to 6.75 kA), the interruption time is reduced by 7.06% (from 7.43 ms to 6.45 ms), and the recovery time of discharging and reversing the capacitor is reduced by 74.39% (from 2.52 ms to 0.37 ms).

Table 5. Results of the optimal parameters for the HCB

Component (Unit)	Initial Parameters	Optimized Parameters	Reducing (%)
I_{pk} (kA)	7.56	6.75	5.66
T_{int} (ms)	7.43	6.45	7.06
T_{rec} (ms)	2.52	0.37	74.39

5. Conclusions

An MOGA-based optimization model using the weighted sum method to find the best design parameters with high performance for the HCB topology has been proposed. This work has considered the three objective functions of peak fault current, interruption time, and recovery time. The simulation results confirm that the optimal values of HCB parameters are found without affecting the overall performance of the HCB. Moreover, a comparison study of the HCB topology with initial and optimal parameters has also been carried out. The proposed work using the HCB with optimal parameters outperforms the previous work using the existing HCB parameters. Clearly, the optimal value of the HCB parameters in this work is smaller than the existing parameters in the previous study, which leads to the size of the passive elements in the HCB topology being reduced by the MOGA application. In addition, compared to the reference parameters, the operation of the HCB using the optimized parameters can significantly reduce the magnitude of the peak fault current by 5.66%, the interruption time by 7.06%, and the recovery time by 74.39%. It can be concluded that the use of the MOGA to optimize the HCB parameters not only reduces the size and cost of the HCB, but also improves the overall service reliability of the entire HVDC system while also mitigating the damage caused by fault currents.

Author Contributions: Conceptualization, V.-V.N.; methodology, V.-V.N. and V.-H.B.; formal analysis, V.-V.N.; investigation, V.-V.N., N.-T.N., and Q.-T.N.; writing—original draft preparation, V.-V.N. and V.-H.B.; writing—review and editing, V.-V.N., V.-H.B. and W.S. All authors have read and agreed to the published version of the manuscript.

Funding: This research received no external funding.

Institutional Review Board Statement: Not applicable.

Informed Consent Statement: Not applicable.

Data Availability Statement: Not applicable.

Conflicts of Interest: The authors declare no conflicts of interest.

References

1. Flourentzou, N.; Agelidis, V.G.; Demetriades, G.D. VSC-based HVDC power transmission grids: An overview. *IEEE Trans. Power Electron.* **2009**, *24*, 592–602.
2. Deng, F.; Chen, Z. Operation and control of a dc-grid offshore wind farm under dc transmission grid faults. *IEEE Trans. Power Del.* **2013**, *28*, 1356–1363.
3. Akhmatov, V.; Callavik, M.; Franck, C.M.; Rye, S.E.; Ahndorf, T.; Bucher, M.K.; Muller, H.; Schettler, F.; Wiget, R. Technical guidelines and prestandardization work for first HVDC grids. *IEEE Trans. Power Del.* **2014**, *29*, 327–335.
4. Bucher, M.K.; Franck, C.M. Contribution of fault current sources in multiterminal HVDC cable networks. *IEEE Trans. Power Del.* **2013**, *28*, 1796–1803.
5. Franck, C.M. HVDC circuit breakers: A review identifying future research needs. *IEEE Trans. Power Del.* **2011**, *26*, 998–1007.
6. Chen, Z. Analysis and experiments for IGBT, IEGT, and IGCT in hybrid DC circuit breaker. *IEEE Trans. Ind. Electron.* **2018**, *65*, 2883–2892.
7. Benfatto, I.; Maschio, A.; Manganaro, S. DC breaking tests up to 55 kA in a single vacuum interrupter. *IEEE Trans. Power Del.* **1988**, *3*, 1732–1738.
8. Eriksson, T.; Backman, M.; Halen, S. A low loss mechanical HVDC breaker for HVDC grid applications. In Proceedings of the CIGRE Session, Paris, France, 24 August 2014; Paper B4-303.
9. Shi, Z.Q.; Zhang, Y.K.; Jia, S.L.; Song, X.C.; Wang, L.J.; Chen, M. Design and numerical investigation of a HVDC vacuum switch based on artificial current zero. *IEEE Trans. Dielectr. Elect. Insul.* **2015**, *22*, 135–141.
10. Kempkes, M.; Roth, I.; Gaudreau, M. Solid-state circuit breakers for medium voltage dc power. In Proceedings of the 2011 IEEE Electric Ship Technologies Symposium, Alexandria, VA, USA 10–13 April 2011; pp. 254–257.
11. Jang, H.-J.; Lee, W.-Y.; Park, S.; Chong, J.-K. A configuration concept of solid-state switch for 2kV class DC circuit breaker. In Proceedings of the 2015 3rd International Conference on Electric Power Equipment—Switching Technology (ICEPE-ST), Busan, Korea, 25–28 October 2015; pp. 435–437.
12. Meyer, C.; Kowal, M.; De Doncker, R.W. Circuit breaker concepts for future high-power dc-applications. In Proceedings of the Fourtieth IAS Annual Meeting. Conference Record of the 2005 Industry Applications Conference, Hong Kong, China, 2–6 October 2005; Volume 2, pp. 860–866.

13. Sano, K.; Takasaki, M. A surgeless solid-state DC circuit breaker for voltage-source-converter-based HVDC systems. *IEEE Trans. Ind. Appl.* **2014**, *50*, 2690–2699.
14. Van Gelder, P.; Ferreira, J.A. Zero volt switching hybrid DC circuit breakers. In Proceedings of the Conference Record of the 2000 IEEE Industry Applications Conference. Thirty-Fifth IAS Annual Meeting and World Conference on Industrial Applications of Electrical Energy (Cat. No.00CH37129), Rome, Italy, 8–12 October 2000; Volume 5, pp. 2923–2927.
15. Bösche, D.; Wilkening, E.-D.; Köpf, H.; Kurrat, M. Breaking performance investigation of hybrid DC circuit breakers: An Experimental Approach. In Proceedings of the 2015 IEEE 61st Holm Conference on Electrical Contacts (Holm), San Diego, CA, USA, 11–14 October 2015; pp. 117–123.
16. Bösche, D.; Wilkening, E.-D.; Köpf, H.; Kurrat, M. Hybrid DC circuit breaker feasibility study. *IEEE Trans. Compon. Packag. Manuf. Technol.* **2017**, *7*, 354–362.
17. Häfner, J.; Jacobson, B. Proactive Hybrid HVDC Breakers—A key innovation for reliable HVDC grids. In Proceedings of the CIGRE Bologna Symposium—The Electric Power System of the Future: Integrating Supergrids and Microgrids, Bologna, Italy, 13–15 September 2011, pp. 1–9.
18. Davidson, C.C.; Whitehouse, R.S.; Barker, C.D.; Dupraz, J.-P.; Grieshaber, W. A new ultra-fast HVDC circuit breaker for meshed dc networks. In Proceedings of the 11th IET International Conference on AC and DC Power Transmission, Birmingham, UK, 10–12 February 2015; pp. 1–7.
19. Wu, Y.; Hu, Y.; Wu, Y.; Rong, M.; Yi, Q. Investigation of an active current injection DC circuit breaker based on a magnetic induction current commutation module. *IEEE Trans. Power Deliv.* **2018**, *33*, 1809–1817.
20. Sander, R.; Suriyah, M.; Leibfried, T. Characterization of a countercurrent injection-based HVDC circuit breaker. *IEEE Trans. Power Electron.* **2018**, *33*, 2948–2956.
21. Nguyen, V.-V.; Son, H.-I.; Nguyen, T.-T.; Kim, H.-M.; Kim, C.-K. A novel topology of hybrid HVDC circuit breaker for VSC-HVDC application. *Energies* **2017**, *10*, 1675.
22. Liu, L.; Liu, S.; Popov, M. Optimized algorithm of active injection circuit to calibrate DC circuit breaker. *Int. J. Electr. Power Energy Grid* **2018**, *103*, 369–376.
23. Liu, Y.; Zhan, X.; Li, R. Optimization design and application of converter parameters of DC vacuum circuit breaker. In Proceedings of the 2017 20th International Conference on Electrical Machines and Grids (ICEMS), Sydney, Australia, 11–14 August 2017; IEEE: Piscataway, NJ, USA.
24. Liu, X.; Yu, D.; Zou, J.; Liao, M. The Multi-objective optimization design of commutation circuit in DC vacuum circuit breaker. In Proceedings of the 2014 International Symposium on Discharges and Electrical Insulation in Vacuum (ISDEIV), Mumbai, India**,** 28 September–3 October 2014; IEEE: Piscataway, NJ, USA.
25. Wen, W. Research on a current commutation drive circuit for hybrid DC circuit breaker and its optimisation design. *IET Gener. Transmiss. Distrib.* **2016**, *10*, 3119–3126.
26. Shabir, S.; Singla, R. A comparative study of genetic algorithm and the particle swarm optimization. *Int. J. Electr. Eng.* **2016**, *9*, 215–223.
27. Lin, C.D.; Anderson-Cook, C.M.; Hamada, M.S.; Moore, L.M.; Sitter, R.R. Using Genetic Algorithms to Design Experiments: A Review. *Qual. Reliab. Engng. Int.* **2014**, *31*, 155–167.
28. Conseil international des grands réseaux électriques. (Ed.). *Technical Requirements and Specifications of State-of-the-Art HVDC Switching Equipment*; CIGRÉ: Paris, France, 2017; ISBN 978-2-85873-386-6.
29. Murata, T.; Ishibuchi, H. MOGA: Multi-objective genetic algorithms. In Proceedings of the 1995 IEEE International Conference on Evolutionary Computation, Perth, WA, Australia, 29 November–1 December 1995; pp. 289–294.
30. Liu, S.; Popov, M. Development of HVDC System-Level Mechanical Circuit Breaker Model. *Int. J. Electr. Power Energy Syst.* **2018**, *103*, 159–167.
31. Greenwood, A.; Lee, T. Theory and Application of the Commutation Principle for HVDC Circuit Breakers. *IEEE Trans. Power Appar. Syst.* **1972**, *PAS-91*, 1570–1574.
32. Kontos, E.; Pinto, R.T.; Rodrigues, S.; Bauer, P. Impact of HVDC transmission system topology on multiterminal DC network faults. *IEEE Trans. Power Deliv.* **2015**, *30*, 844–852.
33. Liu, G.; Xu, F.; Xu, Z.; Zhang, Z.; Tang, G. Assembly HVDC breaker for HVDC grids with modular multilevel converters. *IEEE Trans. Power Electron.* **2017**, *32*, 931–941.